Eleventh International Conference on Computational Fluid Dynamics (ICCFD11), Barcelona, Spain, July 11-15, 2022

ICCFD11-1601

Comparative Assessment of Accuracy of Shock-Capturing Schemes in Terms of Local-Truncation-Error

Yoonpyo Hong*, Soo Hyung Park** and Kwanjung Yee*
Corresponding author: kjyee@snu.ac.kr

* Seoul National University, Republic of Korea
** Konkuk University, Republic of Korea

Abstract: Excessive numerical dissipation, which is considered an inherent limitation of the CFD method, dissipates the physical phenomena, weakens their intensity, and even makes them invisible. Especially in vortex-dominated compressible flowfields such as rotorcraft flowfields, accurate prediction of performance is difficult because numerous vortices effective to aerodynamic performance vanish due to the numerical dissipation. Shock-capturing scheme of low numerical dissipation can be an adequate approach for precise prediction. However, shock-capturing schemes do not promise the same performance in the discretized domain, even if they have the same theoretical accuracy. This is because the non-linear part of each scheme locally deteriorates the accuracy according to grid quality and flow characteristics. Therefore, it is necessary to assess each scheme in terms of local accuracy and identify which characteristics are required for accurate prediction. In this study, a local-order-of-accuracy index (LAI) is used to quantitatively measure the actual accuracy of spatial discretization scheme. The LAI consists of the product and sum of n^{th}-order error measures, which can be calculated through dot product of two vectors: 1) the truncation error coefficient of each stencil, and 2) the polynomial weight of each spatial scheme. Through several benchmark tests, the LAI analysis indicates two requisites for accurate and efficient prediction: 1) a sophisticated non-linear function inherent in each scheme, and 2) hybrid central-upwind characteristics.

Keywords: Shock-Capturing Schemes, Local-order-of-accuracy, Truncation error

1 Introduction

In computational fluid dynamics (CFD) solvers for compressible flow, shock-capturing schemes are essential to deal with the discontinuity such as shock. Shock-capturing schemes robustly yield the calculation results by applying appropriate numerical dispersion to the region with the discontinuity. Total variation diminishing (TVD) – type [1] and total variation bounded (TVB) – type [2] schemes are representative shock-capturing schemes that produce notable results in compressible flow.

As computing power gradually developed, and at the same time, the demand for CFD analysis for complex flows, including the discontinuity, increased, high-fidelity analysis began to be required. Because conventional shock-capturing schemes were only focused on dealing with the shock, there is a limit to producing a calculation result of high accuracy. The excessive numerical dissipation of conventional shock-capturing schemes significantly lowers the accuracy of numerical results. Accordingly, improved shock-capturing scheme which can produce high-accurate results with low

numerical dissipation began to be developed. As the representative improved schemes, weighted essentially non-oscillatory (WENO) - type schemes [3-5] have successfully analyzed the compressible flowfield. They even began to be used in aerodynamic noise areas such as blade-vortex interaction (BVI) dominant rotorcraft flowfield [6,7]. As another concept scheme, there is an enhanced multi-dimensional limiting process (eMLP) – type scheme [8,9] that complements the TVD-type scheme. One of the eMLP-type scheme, the recently developed eMLP-VC scheme, showed time-efficient and high-accurate performance compared to conventional high-order schemes. [9]

However, even with schemes of the same accuracy, the shock-capturing schemes produce completely different results in the same flow field. In fact, as shown in Hong et al., the amounts of physical quantities preserved in the same grid and same conditions is very different depending on the numerical scheme [9]. This can completely different predictions in aerodynamic and aeroacoustic performance.

The main factor that shock-capturing schemes of the same theorical accuracy show different accuracy is the non-linear function in each scheme. The original role of this function is to robustly deal with discontinuity. The problem arises when this function work where discontinuity does not exist. If the grid quality is poor or the flow changes rapidly, the scheme can erroneously consider a discontinuity. This brings unnecessary numerical dissipation and deteriorates the local accuracy. For more efficient and accurate performance prediction, the shock-capturing scheme should have theoretical accuracy in as many domains as possible. Therefore, in this study, local truncation error analysis was conducted to analyze the local accuracy expressed in each flowfield. The essential requirements of shock-capturing scheme were examined for precise prediction of aerodynamic performance.

2 A brief review of shock-capturing schemes

As conventional shock-capturing schemes, designed to capture the discontinuity in the robust manner, the TVD-type and TVB-type schemes give remarkable results. They have successfully captured the shock discontinuity, and dramatically increased the stability of the compressible solver. However, the numerical dissipation of schemes greatly reduces the accuracy of computing results in the incompressible region. To compensate for this problem, researchers presented an enhanced version of each type of scheme. In this study, among the schemes of TVB-type, WENO-type schemes [3-5] were selected, which efficiently improved the accuracy problem. In addition, among the schemes of TVD-type, the enhanced multi-dimensional limiting process (eMLP)-type schemes [8,9] was selected, which uses independent flow-distinguishing-step. All schemes to be compared in this paper are explicit upwind type schemes with fifth-order accuracy.

For both types of schemes, a pure polynomial scheme is applied in the continuous area. In the discontinuous region, the region with the discontinuity such as a shock, numerical dissipation is applied. The method of applying the numerical dissipation is called the non-linear function of each scheme. The non-linear function of each scheme will be summarized in Section 2.

2.1 Non-linear functions in WENO-type schemes

Developed by Jiang and Shu in 1995, WENO-JS [3] is a method of reconstructing the cell interface value by comparing the smoothness of local polynomials. Through the comparison, WENO-JS can reconstruct the cell interface value with high-order accuracy, avoiding the area with a shock discontinuity. For more detailed algorithm, please refer to Jiang and Shu [3]. However, WENO-JS has a problem with reduced accuracy in local extrema. Improved schemes such as WENO-M [4] and WENO-Z [5] have also been developed to complement the reduced accuracy in local extrema.

The non-linear function of the WENO-type is an algorithm that determines the weight of the local polynomial. If the ideal weight is applied, the scheme turns to a pure polynomial scheme. The weight determination algorithm of original WENO (WENO-JS) is as follows:

$$q_{\frac{1}{2}} = \sum_{i=0}^{r-1} w_i^r a_i^r(\bar{q}_{i-r+1}, \dots, \bar{q}_i) \tag{1-a}$$

$$\beta_i^r = \sum_{m=0}^{r-1} \left(\sum_{j=0}^{r-1} s_{imj}^r \bar{q}_{-r+i+j+1} \right)^2 \tag{1-b}$$

$$w_i^r = \frac{\bar{w}_i^r}{\sum_{i=0}^{r-1} \bar{w}_i^r}, \qquad \bar{w}_i^r = \frac{\gamma_i^r}{\left(\epsilon + \beta_i^r\right)^2} \tag{1-c}$$

where $q_{\frac{1}{2}}$ stands for the cell interface value. a_i^r stands for r^{th} order local polynomial. β_i^r means the smoothness indicator for the local polynomial. Finally, the weight of the local polynomial can be obtained as Eq. 1c. ϵ, a small positive number, is set as 10^{-6} in this study.

WENO-M [4], one of the improved WENO-type schemes, designed to preserve high-order accuracy in local extrema, corrects the weight as follows:

$$w_{i,WENO-M}^r = \frac{w_i^r\{\gamma_i^r + (\gamma_i^r)^2 - 3\gamma_i^r w_i^r + (w_i^r)^2\}}{\left(\gamma_i^r\right)^2 + w_i^r\left(1 - 2\gamma_i^r\right)} \tag{2}$$

WENO-Z [5], another improved version, corrects the weight as follows:

$$\tau_{2r-1} = \begin{cases} |\beta_0^r - \beta_{r-1}^r|, & mod(r,2) = 1 \\ |\beta_0^r - \beta_1^r - \beta_{r-2}^r + \beta_{r-1}^r|, & mod(r,2) = 0 \end{cases} \tag{3a}$$

$$w_{i,WENO-Z}^r = \frac{\bar{w}_{i,WENO-Z}^r}{\sum_{i=0}^{r-1} \bar{w}_{i,WENO-Z}^r}, \quad \bar{w}_{i,WENO-Z}^r = \gamma_i^r\left(1 + \frac{\tau_{2r-1}}{\beta_i^r + \varepsilon}\right) \tag{3b}$$

Each weight correction equation acts as a non-linear function of each scheme.

2.2 Non-linear functions of eMLP-type schemes

In eMLP-type schemes [8,9], independent flow-distinguishing-step is used to compensate the excessive numerical dissipation of TVD-type scheme. In this step, the physical characteristics of the flowfield are identified by using a Gibbs phenomenon. Then, according to the physical characteristics, the different reconstruction methods are applied. In the continuous region, the pure polynomial scheme is applied. In the discontinuous region, the TVD or MLP scheme is applied. Applying different reconstruction methods makes numerical dissipation be effectively applied. Also, the improved version of eMLP scheme, eMLP-VC, was also recently developed considering the characteristics of the vortex-dominated flowfield by Hong et al. [9]. eMLP-VC has been applied to various vortex-dominated flowfields, including rotorcraft flowfields, to produce time-efficient and high-accurate results.

A non-linear function of eMLP-type scheme is a mechanism for shock sensing, which is also previously called as flow-distinguishing-step. If the shock-sensor mechanism determines that there is no shock in the local region, eMLP-type scheme applies the pure polynomial reconstruction to that region. Otherwise, eMLP-type scheme applies the TVD scheme or MLP scheme to deal with the shock discontinuity. The accuracy of eMLP-type scheme depends on the shock-sensing performance of the shock-sensor mechanism. The shock sensing mechanism of eMLP and eMLP-VC is represented in Table 1. At the same time, Table 1 plays a role as the non-linear functions of the eMLP-type schemes.

Table 1 Summary of eMLP-type shock-sensoring algorithms ($\epsilon_{eMLP-type} = 0.01$)

Region	Distinguishing criterion	
	eMLP [8]	eMLP-VC [9]
Continuous (pure polynomial reconstruction)	$d_{(\rho,u,v,w,p),i} = \frac{\lvert(\rho,u,v,w,p)_{i,approximate} - (\rho,u,v,w,p)_i\rvert}{\lvert q_i\rvert} < \epsilon_{eMLP-type}$	$d_{(\rho,p),i} = \frac{\lvert(\rho,p)_{i,approximate} - (\rho,p)_i\rvert}{\lvert(\rho,p)_i\rvert} < \epsilon_{eMLP-type}$
Linear discontinuous (TVD reconstruction)	$d_{\rho,i} = \frac{\lvert\rho_{i,approximate} - \rho_i\rvert}{\lvert\rho_i\rvert} > \epsilon_{eMLP-type}$ or $d_{(u,v,w),i} = \frac{\lvert(u,v,w)_{i,approximate} - (u,v,w)_i\rvert}{\lvert(u,v,w)_i\rvert} > \epsilon_{eMLP-type}$	$d_{\rho,i} = \frac{\lvert\rho_{i,approximate} - \rho_i\rvert}{\lvert\rho_i\rvert} > \epsilon_{eMLP-type}$
Nonlinear discontinuous (MLP reconstruction)	$d_{p,i} = \frac{\lvert p_{i,approximate} - p_i\rvert}{\lvert p_i\rvert} > \epsilon_{eMLP-type}$	$d_{p,i} = \frac{\lvert p_{i,approximate} - p_i\rvert}{\lvert p_i\rvert} > \epsilon_{eMLP-type}$

In addition, eMLP-VC has a low-Mach-number adjustment step for the accuracy of subsonic region, which is also included in the non-linear function. Through the low-Mach-number adjustment step, the eMLP-VC could have a hybrid central-upwind characteristic in subsonic region. For more information, please refer to Hong et al. [9,10]

3 Introduction of a local-order-of-accuracy index (LAI) and its application in benchmark test problems

3.1 Local-order-of-accuracy index (LAI)

The accuracy of the shock-capturing scheme, including the above-mentioned schemes, is different according to the characteristics of the flowfield and grid quality due to the non-linear function inherent in each scheme. In other words, in order to analyze non-linear characteristics of shock-capturing schemes, an analysis method that can consider flowfield characteristics and grid quality is needed. Recently, the analysis using LAI suggested by Hong et al.[10] showed the distribution of local truncation error of the spatial discretization scheme, allowing the non-linear characteristics of the scheme to be analyzed. In this paper, the characteristics of shock-capturing schemes will be analyzed through two benchmark tests using LAI.

LAI is an indicator of the local-order-of-accuracy of each scheme in the discretized domain. It consists of the truncation error and the stencil weight expressed through Taylor series expansion. LAI for fifth-order spatial schemes can be defined as follows [10]:

$$LAI = 1 + \sum_{k=1}^{5} \prod_{i=1}^{k} \left(1 - \frac{\lvert \boldsymbol{c^T} \cdot \boldsymbol{e_i} \rvert}{\lvert \Gamma_i \rvert}\right) = 1 + \left(1 - \frac{\lvert \boldsymbol{c^T} \cdot \boldsymbol{e_1} \rvert}{\lvert \Gamma_1 \rvert}\right) + \left(1 - \frac{\lvert \boldsymbol{c^T} \cdot \boldsymbol{e_1} \rvert}{\lvert \Gamma_1 \rvert}\right)\left(1 - \frac{\lvert \boldsymbol{c^T} \cdot \boldsymbol{e_2} \rvert}{\lvert \Gamma_2 \rvert}\right) + \cdots + \left(1 - \frac{\lvert \boldsymbol{c^T} \cdot \boldsymbol{e_1} \rvert}{\lvert \Gamma_1 \rvert}\right)\left(1 - \frac{\lvert \boldsymbol{c^T} \cdot \boldsymbol{e_2} \rvert}{\lvert \Gamma_2 \rvert}\right) \cdots \left(1 - \frac{\lvert \boldsymbol{c^T} \cdot \boldsymbol{e_5} \rvert}{\lvert \Gamma_5 \rvert}\right) \tag{4}$$

where Γ_i stands for a constant for normalizing $\lvert \mathbf{c^T} \cdot \boldsymbol{e_i} \rvert$ and $\boldsymbol{e_i}$ stands for i^{th}-order truncation error coefficients. The coefficients of shock-capturing schemes, $\boldsymbol{c}$, can be rewritten as:

$$\boldsymbol{c_{WENO-type}} = \frac{1}{6}\,(2w_0, -7w_0 - w_1, 11w_0 + 5w_1 + 2w_2, 2w_1 + 5w_2, -w_2\,, 0)^T \tag{5a}$$

$$\boldsymbol{c_{eMLP-type,continuous}} = \frac{1}{60}(2 - g, 5g - 13, 47 - 10g, 27 + 10g, -3 - 5g, g)^T \tag{5b}$$

$$\boldsymbol{c_{eMLP-type,discontinuous}} = f_{LM}\left(c_{-2}(\phi), c_{-1}(\phi), c_0(\phi), c_1(\phi), c_2(\phi), c_3(\phi)\right)^T \quad (5c)$$

Coefficients of the fifth-order WENO-type scheme can be expressed as in Eq. 5a. $w_j(j = 0,1,2)$ means the weights of local polynomials shown in Eq. 1. Coefficients of fifth-order eMLP-type schemes can be expressed as Eq. 5b-c. The coefficients of the continuous region can be expressed by the fifth-order accurate polynomial reconstruction and the low Mach number adjustment function, g. In the discontinuous region, it can be expressed as a function of TVD and MLP, ϕ. LAI is applied to compare the capabilities of non-linear functions of these schemes in the discretized domain. For more information about LAI, please refer to Hong et al. [10].

3.2 A one-dimensional numerical test

As one-dimensional benchmark test, a smooth sine wave advection test was conducted. The initial condition is as follows:

$$q = 6 + 5\left(\sin\left(\frac{\pi}{2.5}x\right)\right)$$

An upwind scheme was applied as the flux scheme. The 3rd order TVD Runge-Kutta scheme was applied for temporal integration method. In the fine grid system, all schemes determine that the area is continuous and produce 5th order accuracy. Therefore, this test was conducted with a coarse grid system to compare the difference of the performances of shock-capturing schemes. The domain is composed of [-5,5] with equally spaced grids. 21 grid points are used. This can be seen in Figure 1a.

LAI distribution in all domains is presented in Figure 1b. For ease of comparison, the results of the fifth- and sixth-order accurate polynomial reconstruction were also plotted. All shock-capturing schemes claim that they have fifth-order accuracy. But the LAI distributions shows that shock-capturing schemes do not have fifth-order accuracy locally in the discretized domain.

The error measure of each scheme is represented in Figure 2. The legends in Figure 2 are all the same as the legends in Figure 1b. In the case of WENO-type, WENO-JS has the largest third- and fourth-order error measures in all domain. On the other hand, WENO-M and WENO-Z have almost the same error level. The weight functions of WENO-M and WENO-Z are more sophisticated than that of WENO-JS, indicating that the error level is low. When eMLP-type schemes are used, the entire area is determined to be a continuous area in the current problem. Therefore, there are no third- and fourth-order error measures. On the other hand, in the case of a fifth-order error measure, all schemes except for eMLP-VC approach the error level, 1. It is mainly due to the low Mach number adjustment step inherent in eMLP-VC, which has dramatically reduced the fifth-order error measure.

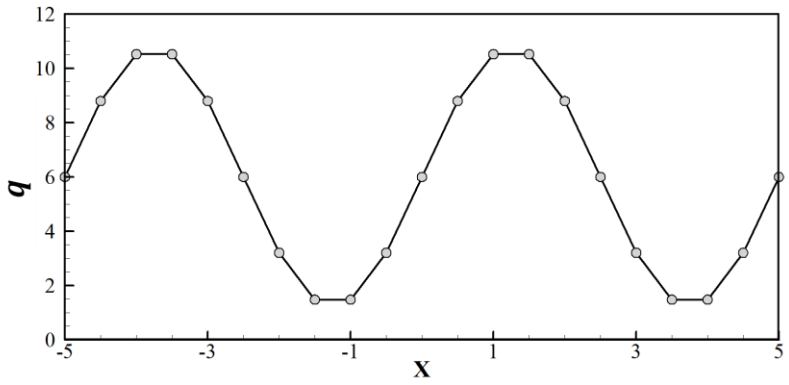

a) Sine wave profile ($q = 6 + 5\sin\left(\frac{\pi}{2.5}x\right)$)

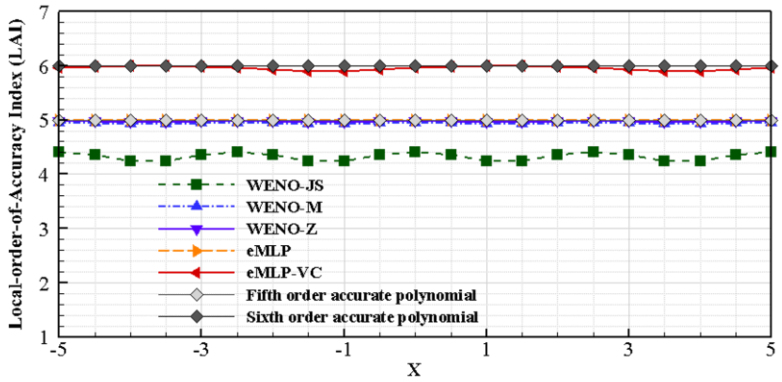

b) Local-order-of-accuracy index (LAI) distributions

Figure. 1 Sine wave profile and local-order-of-accuracy index distributions of numerical schemes.

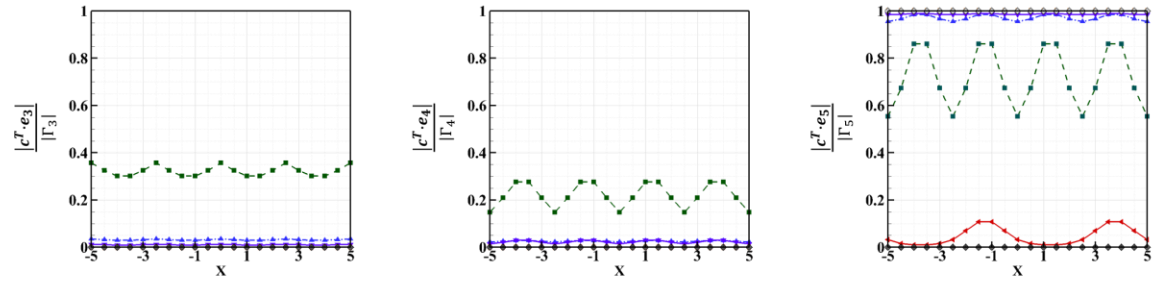

a) Third-order error measure *b*) Fourth-order error measure *c*) Fifth-order error measure

Figure. 2 Error measure of numerical schemes in sine wave advection problem.

3.3 A two-dimensional numerical test

The shock-vortex interaction problem was selected as a two-dimensional test of complex compressible flowfield[?]. This problem is suitable for comparing the robustness and accuracy of the applied numerical scheme. Reynolds-averaged Navier-Stokes equations were set as a governing equation. The Reynolds number is set as 800. The shock moves from right to left with 1.29 Mach number. The stationary vortex is defined by the following equation.

$$\left(\rho_0, u_{\theta,0}, u_{r,0}, p_0\right) = \left[\left\{1 - \frac{\gamma - 1}{2} M_v^2 \exp[1 - r_v^2]\right\}^{\frac{1}{\gamma - 1}}, M_v r_v \exp\left[\frac{1 - r_v^2}{2}\right], 0, \frac{\rho_0^\gamma}{\gamma}\right]$$

where ρ_0 stands for the initial density. p_0 is the initial pressure. $u_{\theta,0}$ and $u_{r,0}$ mean the tangential and radial velocities, respectively. The vortex Mach number, M_v is set as 0.39. r_v stands for the distance from the stationary vortex core $(x, y) = (0,0)$. The upwind-type flux scheme, AUSMPW+ [12], was used as the flux function. As time integration method, 3rd order TVD Runge-Kutta scheme was used. A very small time-interval was set to minimize the temporal error. The computational domain was composed of [-20, 8] × [-12, 12] with equally spaced grids. The number of grids for comparison is 140×120. A very dense grid system 1120×960 was used to obtain the reference result.

Figure 3 is the flowfield of shock-vortex interaction problem using the reference grid system and eMLP-VC scheme. The flowfield was shown using numerical schlieren. It is expressed according to non-dimensionalized time, *t*. The details of interaction between the shock and the vortex are represented.

When non-dimensionalized time, *t* is 13, the LAI contours of five different shock-capuring schemes are shown in Figure 4. Because WENO-type and eMLP schemes produce up to 5th order accuracy, the overall contour color appears dark. On the other hand, the accuracy of eMLP-VC result has increased because low-Mach-number adjustment was conducted in most areas except for the shock discontinuity are subsonic. In Figure 4, the effects of vortex can also be examined. WENO-JS shows low LAI in the region where the shock and the vortex interacts, because it considers that the part of the vortex is discontinuous. Similarly, WENO-M and WENO-Z show numerical dissipation for the part of the vortex areas. On the other hand, eMLP-type schemes apply numerical dissipation only in the area with the shock discontinuity.

Figure 5 shows the pressure distributions along y=0 line when non-dimensionalized time, *t* is 12. Every scheme captures the shock discontinuity in a robust manner. In the case of vortex after the interaction with shock, the trend of vorticity preserved was very similar to the result of LAI analysis. The vortex pressure was most preserved by eMLP-VC. Improved WENO-type schemes had higher vortex preserving capability than original WENO, WENO-JS.

As a result, two conclusions can be summarized for high-accurate numerical results. First, the shock-capturing schemes should have ideal accuracy in as many areas where there is no discontinuity. To get ideal accuracy in as many areas, the nonlinear function must be sophisticated. Secondly, the shock-capturing schemes should have hybrid central-upwind characteristics in subsonic region. In most cases, eMLP-VC perform the best, because it considers the degradation of accuracy in subsonic area. In subsonic regions, upwind reconstruction should be avoided because of its high numerical dissipation.

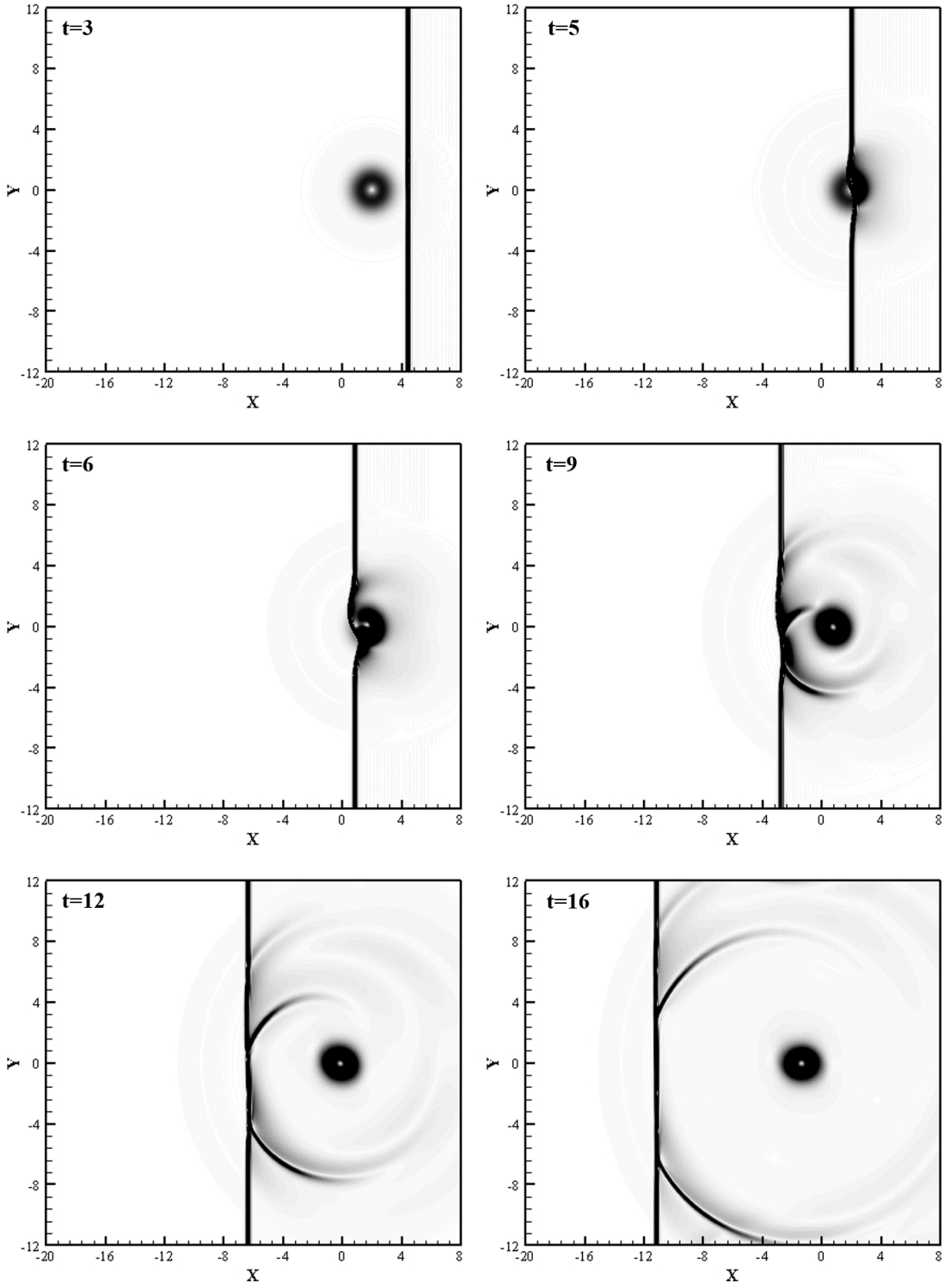

Figure. 3 Numerical schlieren of shock-vortex interaction problem (results of eMLP-VC).

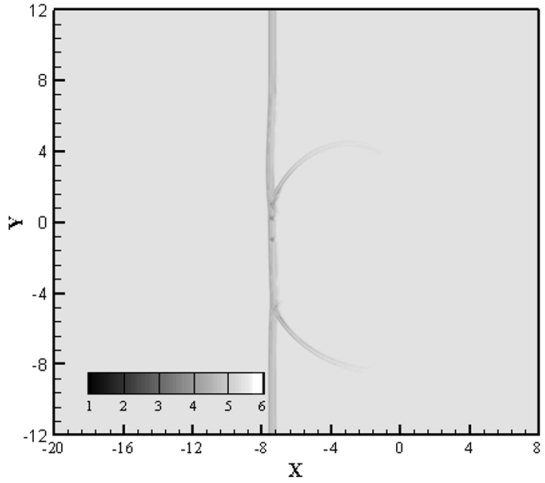

***a*) LAI$_{ressure}$, WENO-JS**

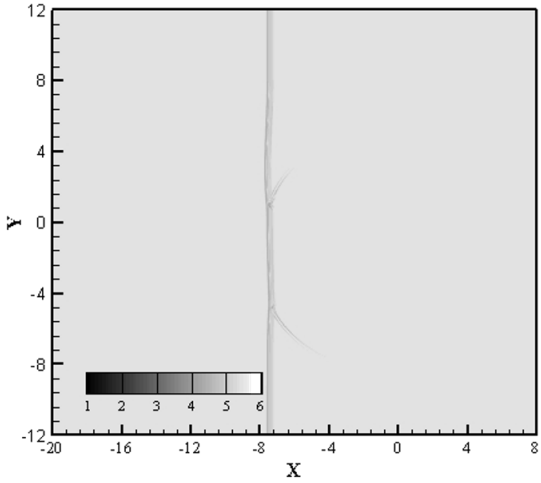

***b*) LAI$_{Pressure}$, WENO-M**

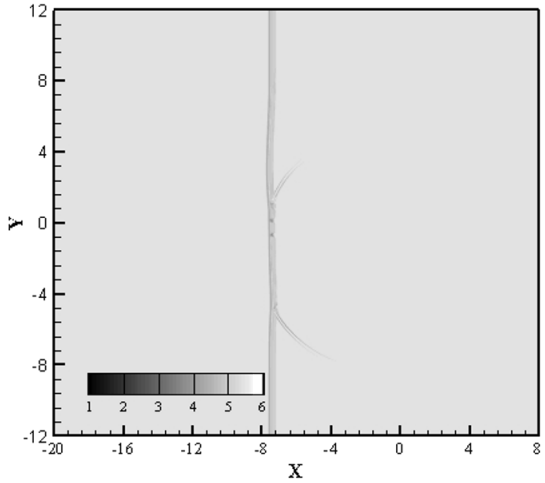

***c*) LAI$_{Pressure}$, WENO−Z**

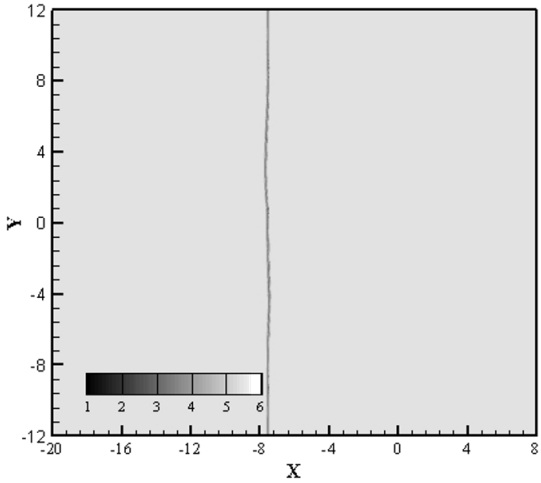

***d*) LAI$_{Pressure}$, eMLP**

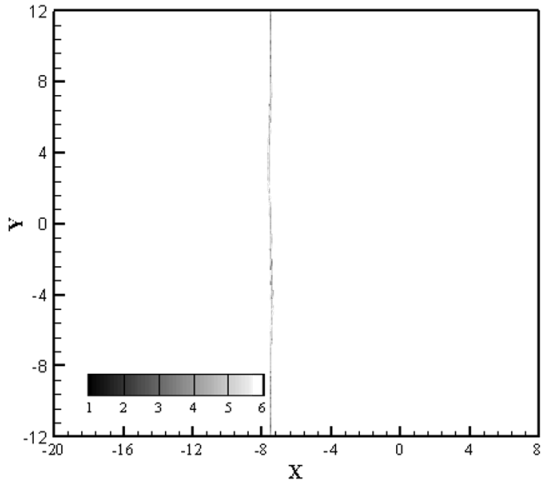

***e*) LAI$_{Pressure}$, eMLP−VC**

Figure. 4 Local-order-of-accuracy index contours of five different numerical schemes.

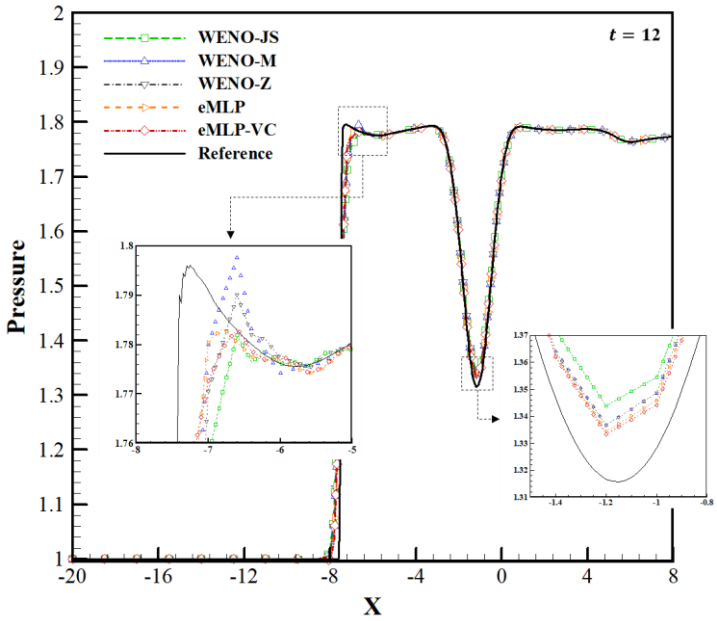

Figure. 5 Pressure distributions of shock-vortex interaction problem (along the line of y=0).

4 Conclusion and Future Work

The local-order-of-accuracy of five shock-capturing schemes was analyzed in one- and two-dimensional benchmark tests for compressible flow. Shock-capturing schemes have locally degraded accuracy in the discretized domain because of the non-linear function that exists to deal with the shock discontinuity. The LAI of each scheme was analyzed, and the pre-requisites that the shock-capturing scheme should have were derived. For future works, a three-dimensional complex engineering problem, such as rotorcraft flowfield, will be solved using five different shock-capturing schemes. The results will be compared and analyzed with the LAI analysis results.

References

[1] Sweby, P. K. "High resolution schemes using flux limiters for hyperbolic conservation laws." *SIAM journal on numerical analysis*, Vol. 21, No. 5, 1984, pp. 995–1011. doi: 10.1137/0721062.
[2] Shu, C.-W., "TVB uniformly high-order schemes for conservation laws," *Mathematics of Computation*, Vol. 49, 1987, pp.105–211.
[3] Jiang, G. S., and Shu., C. W., "Efficient Implementation of Weighted ENO Schemes," *Journal of Computational Physics*, Vol. 126, No. 126, 1996, pp. 202–228. doi: 10.1006/jcph.1996.0130.
[4] Henrick, A. K., Aslam, T. D., and Powers, J. M., "Mapped Weighted Essentially Non-Oscillatory Schemes: Achieving Optimal Order near Critical Points," *Journal of Computational Physics*, Vol. 207, No. 2, 2005, pp. 542–567. doi: 10.1016/j.jcp.2005.01.023.
[5] Borges, R., Carmona, M., Costa, B., and Don, W. S., "An Improved Weighted Essentially Non-Oscillatory Scheme for Hyperbolic Conservation Laws," *Journal of Computational Physics*, Vol. 227, No. 6, 2008, pp. 3191–3211. doi: 10.1016/j.jcp.2007.11.038.
[6] Sa, J. H., You, Y. H., Park, J. S., Jung, S. N., Park, S. H., and Yu, Y. H., "Assessment of CFD/CSD Coupled Aeroelastic Analysis Solution for HART II Rotor Incorporating Fuselage Effects," *American Helicopter Society 67th Annual Forum Proceedings*, 2011, pp. 736–748.
[7] Boyd, D. D., "HART-II Acoustic Predictions Using a Coupled CFD/ CSD Method," *American Helicopter Society 65th Annual Forum Proceedings*, AHS International, Grapevine, TX, May 2009.
[8] Kang, H. M., Kim, K. H., and Lee, D. H., "A New Approach of a Limiting Process for Multi-

Dimensional Flows," *Journal of Computational Physics*, Vol. 229, No. 19, 2010, pp. 7102–7128. doi: 10.1016/j.jcp.2010.06.001.
[9] Hong, Y., Lee, D., and Yee, K. "Enhanced High-Order Scheme for High-Resolution Rotorcraft Flowfield Analysis." *AIAA Journal*, Vol. 60, No. 1, 2022, pp. 144–159. doi: 10.2514/1.J060803.
[10] Hong, Y., Yee, K., and Park, S.H. "Assessment of High-Order Schemes for Vortex-Dominated Flowfield Using Truncation Error Analysis." *AIAA AVIATION 2022 Forum*, 2022. doi: 10.2514/6.2022-4121.
[11] Ellzey, J. L., Henneke, M. R., Picone, J. M., and Oran, E. S., "The Interaction of a Shock with a Vortex: Shock Distortion and the Production of Acoustic Waves," *Physics of Fluids*, Vol. 7, 1995, pp. 172–184
[12] Kim, K. H., and Kim, C., "Accurate, Efficient and Monotonic Numerical Methods for Multi-Dimensional Compressible Flows. Part I: Spatial Discretization," *Journal of Computational Physics*, Vol. 208, No. 2, 2005, pp. 527–569. doi: 10.1016/j.jcp.2005.02.021.